



Supplementary Materials for

Binary interaction dominates the evolution of massive stars

H. Sana, S.E. de Mink, A. de Koter, N. Langer, C.J. Evans, M. Gieles, E. Gosset,
R.G. Izzard, J.-B. Le Bouquin, F.R.N. Schneider

correspondence to: H.Sana@uva.nl

This PDF file includes:

Supplementary Text
Figs. S1 to S4
Tables S1 to S4

Supplementary Text

In these supplementary materials, we provide more details on our O-type star sample, including new orbital constraints for five long period systems. We also provide additional considerations regarding cluster dynamical interaction and stellar evolution, and we argue that these effects do not modify the multiplicity properties of the investigated population. In Section B, we describe observational biases that affect binary detection and the way in which we accounted for them, followed by a description of our Monte Carlo algorithm. We also provide information on the fitting of the orbital parameter distributions and on the behavior of the merit function in the vicinity of the best fit. Finally, Section C presents our calculations of the interaction rates for O-type stars. The notation used throughout the article is defined in Table S1.

A. The observational sample

Since the first survey of massive binaries 30 years ago (10), about three quarters of the Galactic O-type stars within approximately 5 kpc have been observed through multi-epoch spectroscopy. Recent work on a sample of 305 objects reports an observed binary fraction of 50% (11). However only 25% of the identified systems have reliable constraints on their orbital properties (13). This has so far prevented reliable conclusions on the distributions of the orbital distributions to be drawn. Smaller scale studies (16-21) that focused on the O-type population of individual young open clusters observed binary fractions between 30 and 60%. They achieved better completeness in characterizing the identified binaries but the small sample sizes limited the statistical significance of these results. Observed differences between these studies have been suggested to result from small number statistics (13).

To overcome previous limitations due to sample size, we homogeneously analyze the O star population of six Galactic young open clusters with a significant massive star population: IC 1805 (16-17, 32), IC 1848 (17), NGC 6231 (18), NGC 6611 (19), Tr 16 (20) and IC 2944 (21). The clusters were selected because the large majority of their O-type stars have been investigated through multi-epoch spectroscopy and because most of the identified binaries with orbital periods up to two months have been subject to dedicated follow-up to constrain orbital parameters. We have complemented existing observations with a long-term spectroscopic monitoring to constrain the orbital properties of most of the remaining longer period spectroscopic binaries in these clusters (see §A.1).

Our sample clusters contain in total 82 O-type objects, of which 71 have more than five radial velocity (RV) measurements. The remaining 11 objects have two or less RV measurements, which is insufficient for this work; four of these objects with limited RV coverage are spectroscopic binary candidates because of observed variations between the only two observing epochs or because of evidence for double-lined profiles. Finally, 87% of our sample stars are located within 5 to 7 pc from the cluster centers while an

additional nine stars, in IC2944, IC 1848, IC 1805 and Tr 16, are further away from their respective cluster centers.

The 71 single or multiple O-type objects of our sample have been observed through spectroscopy at 1856 epochs in total. Our analysis is thus based on an average of over 20 RV measurements per object that typically span timescales of days, weeks and years, which allows us to attain a large detection probability of the binaries. About three quarters of the detected binaries in these clusters have a well constrained orbit and 85% of the binary systems have a reliable estimate of their orbital period. The O stars in our sample have spectral types ranging from O3 to O9.7, which correspond to a mass range from 15 to 60 solar masses (1).

Counting individually each O star, either single or part of a binary system as a primary or as a secondary component, over half of the O stars in our sample belong to a binary system with a period of less than 1500 days. These stars will either merge or exchange mass with their companion during their lifetime, which suggests, even before correcting for undetected binaries, that binary interaction affects the evolution of the majority of massive stars.

A.1. Orbital properties of our sample binaries

The orbital properties of 29 binaries in our sample have been analyzed in previous studies of which all but one have periods shorter than 50 days. By addition of new UVES observations to existing RV measurements, providing an observational timebase of five to ten years depending on the system, we constrain the orbital properties of an additional five long period systems. We follow the methods described in previous works for data reduction, radial velocity measurements and determination of the orbital properties (18-19, 21). For four systems, detailed orbital solutions can be obtained (Table S2 and Figure S2). For HD168137, our data do not sufficiently sample the periastron passage and therefore uncertainties on the eccentricity remain large ($e > 0.6$). The period is however well constrained by a Fourier analysis (18-19), yielding 912 ± 29 d. We estimate the mass-ratio of these five binaries using a spectral type to mass calibration (1). Table S4 lists the orbital properties of all the binaries in our sample. The full list of 1856 observational epochs and measured RVs, including our new measurements from UVES data, are made available at the Centre de Données astronomiques de Strasbourg (<http://cdsweb.u-strasbg.fr/>).

In total, 34 and 31 of our systems have constrained orbital periods and mass-ratios respectively. Figure S1 shows the positions of the binaries from our cluster sample in the period (P) - mass-ratio (q) - eccentricity (e) parameter space. Our sample populates the P - q and e - q planes homogeneously with no indication of a detection bias against low mass-ratio systems as a function of the orbital period or eccentricity. Short period systems with $P < 4$ days have zero or negligible eccentricity as expected from tidal circularization theory (37).

A.2. Importance of cluster dynamics and stellar evolution effects

Given the young age of the stellar clusters in our sample (1-4 Myr), our derived distributions do well represent natal binary properties. Here we provide two lines of argument showing that dynamical interactions have played a minor role for the majority of the objects. We also briefly discuss the effect of stellar evolution.

We estimate that dynamical interactions with other cluster members are not expected to have significantly altered the orbital properties of the binaries in our sample. Clusters considered here contain typically 500 stars and have half-mass radii of about 5 pc, hence typical densities within the half-mass radii of about $n = 1 \text{ pc}^{-3}$ and root-mean-square velocities $v_{\text{rms}} \approx 200 \text{ m s}^{-1}$. The encounter time-scale, defined as $\tau_{\text{enc}} = (n \pi a^2 v_{\text{rms}})^{-1}$ (ignoring gravitational focussing), where a is the semi-major axis, is $\tau_{\text{enc}} \gtrsim 100 \text{ Myr}$ for binaries with components of 20 solar masses and $a = 10 \text{ AU}$ (corresponding to $P \approx 1000$ days). Further arguments that our binaries are not dynamically active are given in Fujii & Portegies Zwart (38), especially their Fig. 2. In NGC6611, the densest cluster in our sample, binaries with periods well in excess of 1000 days may interact through binary-binary encounters but the shorter period systems that dominate the sample are left unaffected.

Energy considerations also demonstrate that dynamical interactions hardly modify the orbital parameters of our binaries. Any dynamical interaction that could substantially change the orbital parameters would at the same time kick the binary out of the cluster to which it belongs. A massive binary with a period of 1000 days has a binding energy one thousand times that of the kinetic energy of a typical cluster star. Most of our binaries have even shorter-period orbits (i.e. they are harder), and are more tightly bound by up to a factor of 100. Fly-bys and resonant encounters increase the binary binding energy by 20 or 40% respectively (39-40) and one third of this energy goes into the recoil of the center of mass of the binary system. The single star absorbs the remaining two thirds. For the binding energies under consideration, both the binary and the third star would be ejected out of the cluster in the recoil. For the binaries in our stellar clusters, dynamical interactions therefore can only have a minor impact in altering their orbital properties.

Stellar and binary evolution effects also alter the multiplicity properties but typically do not play a significant role in the first 5 Myr (7, 29). They tend to either decrease the binary fraction or lengthen orbital periods. If such effects are important, the number of close binaries at birth is even larger than our estimate and our conclusions are even stronger.

B. On the observational biases of spectroscopic studies

Two main diagnostics identify multiple systems with spectroscopy: Doppler shifts and multiple-lined profiles. Less often, multiplicity is revealed through other spectroscopic diagnostics such as line profile variability. The detection of spectroscopic binaries is inherently biased towards systems displaying a larger RV signal, i.e. edge-on

short-period systems with components of similar mass and/or flux. Small inclination and/or long-period systems generate smaller Doppler displacements and are harder to detect. Furthermore, eccentricity can concentrate the RV signal to only a small fraction of the orbit. Other aspects are highlighted by the equations of the projected orbital velocities of the primary (v_1) and secondary (v_2) stars at a given time t ,

$$v_1(t) = q \left(\frac{2}{1+q} \right)^{2/3} \left(\frac{\pi G M_1}{2P} \right)^{1/3} \sin i \sqrt{1-e^2} (\cos(\phi_{tr} + \omega) + e \cos \omega) \quad (1)$$

and

$$v_2(t) = - \left(\frac{2}{1+q} \right)^{2/3} \left(\frac{\pi G M_1}{2P} \right)^{1/3} \sin i \sqrt{1-e^2} (\cos(\phi_{tr} + \omega) + e \cos \omega), \quad (2)$$

where notations of Table S1 have been used and where the true anomaly, ϕ_{tr} , is a function of the orbital phase $\phi = (t - T) / P$. All other quantities being equal, the RV signature increases with the primary mass. Mass-ratios close to unity enhance the primary RV signal but decrease that of the secondary. A small mass-ratio would favor detection through the orbital motion of the secondary but the flux ratio may become such that the secondary signature is invisible in the composite spectrum. The geometry of the system also plays a role. A smaller inclination decreases the amplitude of the RV signal while random sampling induces a bias against systems with a periastron argument (ω) close to π or 2π . Good orbital sampling, in particular during phases of large RV variations, is critical to improve the chance of detection. Unfortunately, the period and the time of periastron passage are unknown when observations are planned.

In summary, this discussion illustrates two important points: (i) the detection probability of a spectroscopic binary is not equal across the parameter space defined by the orbital elements, (ii) once a system is detected, retrieval of the correct orbital parameters needs a well sampled orbit, typically requiring a variable amount of observational effort depending on the orbital properties. These effects can cause the observed distributions of the orbital parameters to strongly deviate from the intrinsic distributions, in particular in the long orbital period and/or low mass ratio regime. It is thus critical to quantify these observational biases in order to constrain the intrinsic orbital parameter distributions.

B.1. Modelling observational biases

Estimation of the role played by the observational biases is a difficult problem. Their relative impact depends on the distributions of the orbital parameters which are not known a priori. Our approach relies on Monte-Carlo simulations to test sets of intrinsic parameter distributions against our observations while accounting for the observational biases.

In principle, we should consider input distributions for all seven orbital parameters ($P, e, \omega, \sin i, T, M_1, q$) and the intrinsic binary frequency of the sample (f_{bin}). To limit the

number of degrees of freedom that need to be investigated we impose the following assumptions:

1. the orbital plane is randomly oriented in three-dimensional space;
2. the time of periastron passage is uncorrelated with respect to the start of the *RV* campaign;
3. the primary masses are adopted based on a spectral type to mass calibration (1);
4. the orbital parameters are uncorrelated.

Given these hypotheses we use analytical non-parametrized expressions for the probability density functions (*pdf*) of the inclination i , the argument of periastron ω and the time of periastron passage T . We adopt power laws to describe the intrinsic probability density functions for the periods [$pdf(\log_{10} P) \sim (\log_{10} P)^\pi$], mass-ratios [$pdf(q) \sim q^\kappa$] and eccentricities [$pdf(e) \sim e^\eta$]. As a consequence, the problem is reduced to four dimensions: the intrinsic binary fraction (f_{bin}) and the exponents π , κ and η of the three power laws describing $pdf(\log_{10} P)$, $pdf(q)$ and $pdf(e)$.

To compare the observed orbital parameter distributions with our simulations we implement criteria to determine whether a simulated binary is detectable and whether its orbital properties are measurable given the amplitude of the *RV* signal and the observational sampling. We follow the approach of Sana et al. (19) and adopt a threshold $C = 20 \text{ km s}^{-1}$ for the observed primary *RV* amplitude (Δv_1) such that the binary detection criterion is given by $\Delta v_1 > C$. We focus on the primary orbital motion so that the single-lined and double-lined systems can be treated homogeneously.

Whether orbital properties are measurable depends on the nature of the considered systems and associated *RV* measurements. To deal with the decision-making involved in binary detection and orbit determination we employ the following reasoning. While it is possible to detect a binary with only a few observational epochs, it is highly improbable that a reliable orbit is obtained. Conceptually, there is a critical minimum number of observations (n_{crit}) from which it is possible to reliably constrain an orbit. A representative value of n_{crit} can be obtained from our data set: the minimum number of observations associated with a published orbit is nine and all systems but one with at least 14 observations have constrained orbits. We tested the dependence of our results on values of n_{crit} between 10 and 15 and found no significant impact, hence we adopt $n_{\text{crit}} = 12$ as representative of our sample.

Following the observational limitations and the properties of our data set, we assume that mass-ratios below 0.2 and eccentricities larger than 0.7 cannot be measured. It is not possible to a priori decide whether the absence of systems with such properties is due to observational biases or whether the parent parameter distributions are effectively truncated. Because $q \sim 0.2$ and $e \sim 0.7$ correspond to effective observational limits (13), the first option is more likely. The ranges of mass-ratios and eccentricities considered are thus 0.1-1.0 and 0.0-0.9 respectively (Table S3) while the range of periods considered is $0.15 < \log_{10}(P/\text{day}) < 3.5$, in agreement with the periods measured from our sample.

B.2. Monte Carlo algorithm

Let us consider an observed sample of N objects, each with n_i observations ($i = 1 \dots N$) obtained at times $t_{k,i}$ ($k = 1 \dots n_i$). By adoption of a distribution for $\log_{10} P$, q and e and a binary fraction f_{bin} , we generate synthetic populations of massive stars and compare them with the observational sample as follows:

1. We adopt a population of N objects and assign to each of them a mass and an observational sampling $\{t_{k,i}\}_{k=1}^{n_i}$ taken from the observed data set;
2. A binomial statistics with success probability f_{bin} allocates a single or a binary status to each of the synthetic objects;
3. For each binary $\log_{10} P$, q and e are drawn randomly from the tested distributions;
4. The three-dimensional orientation of each orbit and the corresponding time of periastron passage are drawn randomly;
5. Given the orbital parameters and primary masses, the primary RVs of the simulated systems are computed at the epochs corresponding to the observations;
6. The binary detection criterion is applied and the detected systems are flagged: this yields the simulated fraction of detected binaries $f_{\text{obs}}^{\text{simul}}$;
7. The number of observing epochs of the simulated objects complying with the detection threshold $\Delta v_1 > C$ are compared with n_{crit} . If $n_i \geq n_{\text{crit}}$, the orbital period is assumed to be recovered. If $q > 0.2$ and $e < 0.7$, the mass-ratio and eccentricity are, respectively, assumed to be properly measured;
8. The process is repeated 100 times to build up the parent statistics.

By repeating these steps at each point of our four-dimensional mesh (Table S3), we simulate observational cumulative distribution functions (CDFs) for $\log_{10} P$, q and e and for the detected binary fraction. These simulated distributions are compared to the observed CDFs distributions using one-sided Kolmogorov-Smirnov (KS) tests which yield probabilities P_{KS} . The observed binary fraction and the simulated fraction of detected systems are also compared. By use of a binomial distribution we compute the probability $B(N_{\text{bin}}, N, f_{\text{obs}}^{\text{simul}})$ of obtaining N_{bin} detected binaries in a population of N objects given a success probability of $f_{\text{obs}}^{\text{simul}}$. Finally the global merit function (Ξ) is defined as the product of the individual P_{KS} probabilities and $B(N_{\text{bin}}, N, f_{\text{obs}}^{\text{simul}})$.

We perform tests of the method using simulated populations of stars that share the same observational sampling as our data. We adopt flat distributions of the period, mass-ratio and eccentricity (i.e., $\pi = \kappa = \eta = 0$) for various intrinsic binary fractions. For large binary fractions ($f_{\text{bin}} > 0.50$), we recover the input power-law indices in all cases within 0.3. For low binary fractions or whenever the number of detected binaries in our simulated sample drops below 20 objects the uncertainties are large and the method has difficulties in recovering the input distributions. This is especially true when the orbital properties of these 20 binaries fail to sample the full range of the orbital parameter space. With 15 binaries or less, none of our simulations converge to the correct input distributions. Fortunately, this limit is well below the actual number of detected binaries in our sample.

We also explore other intrinsic distributions. We find that Gaussian distributions for the orbital (\log_{10}) period are not as appropriate in reproducing the observations than power laws. The peak probability for the period distribution is a factor two smaller than when using a power law. In order to reproduce the steep rise of the cumulative period distribution up to 10 days, a very small standard deviation is needed ($\sigma \sim 0.6$). As a consequence, such Gaussian distributions cannot reproduce the longer period systems ($P > 100$ days) present in the data. We also test a double Oepik law for the period distribution (13) but find again that simple power laws provide the most appropriate representation of the data.

B.3. Results

Figure S4 shows the projection of the global merit function Ξ on the six two-by-two planes defined by the four degrees of freedom (Table S3). It illustrates two important properties : (i) the merit function Ξ shows a well-defined, smooth and monotonic peak in the investigated ranges; (ii) the power law exponents in $\log_{10} P$, q and e are mostly independent, a posteriori justifying our approach to multiply the P_{KS} probabilities. The period index and the binary fraction show a small degree of correlation that can be understood as follows: large positive values of the exponent π of $pdf(\log_{10} P)$ result in a higher frequency of long period systems. These are harder to detect and an increase in the intrinsic binary fraction is required to match the number of observed binaries in our sample. Similarly, large negative values of π correspond to a large fraction of short-period systems. Because short-period systems are little affected by detection biases the parent binary fraction is closer to the observed fraction. The degeneracy is lifted by simultaneous adjustment of the period distribution and the parent binary fraction, which justifies the introduction of the binomial probability $B(N_{\text{bin}}, N, f_{\text{obs}}^{\text{simul}})$ in our global merit function.

We assess the uncertainties on the derived parent distributions with Monte-Carlo simulations. We generate 40 synthetic populations that share the properties of our sample and are randomly drawn from the best-fit parent distributions, i.e. $f_{\text{bin}} = 0.69$, $\pi = -0.55$, $\kappa = -0.10$, and $\eta = -0.45$. Each synthetic population is input to our code and we re-derive the best-fit intrinsic binary fraction and parent distributions. The mean and 1σ dispersion of the retrieved parameters serve as a check for the presence of systematic biases and as a probe for the accuracy of the procedure. We obtain $\langle f_{\text{bin}} \rangle = 0.74 \pm 0.09$, $\langle \pi \rangle = -0.38 \pm 0.22$, $\langle \kappa \rangle = -0.21 \pm 0.58$ and $\langle \eta \rangle = -0.42 \pm 0.17$. We conclude that the method is unbiased and we adopt the dispersions as uncertainties on the respective parameters of the fit. Similar values are obtained by adopting the confidence interval corresponding to the full width at half-maximum of the global merit function Ξ .

The larger dispersion in η seen in Figure S4 compared to the estimated accuracy of the method may originate from tidal circularization effects that introduce a correlation between the periods and the eccentricities (Fig. S1). We have tested both correlated and uncorrelated functions for the eccentricities. We have also tested a merit function that does not use the eccentricity distribution. In all cases, we observe no significant impact

on the derived binary fraction and distributions of the periods and the mass-ratios. This is in line with the results of Figure S4 that show that the merit function Ξ reacts independently to the various parameter considered. Uncertainties on the correlation between P and e have thus no impact on our results for f_{bin} , π and κ .

Finally, we note that the P_{KS} probabilities for the period and mass-ratio distribution peak above 0.5, suggesting that the simulated distributions shown in Fig. 1 are in good agreement with the observed distributions. The P_{KS} probability for the eccentricity distribution peaks at 0.03, which suggests an imperfect, although still relevant representation of the observed distribution. Whether or not we include $P_{\text{KS}}(e)$ in the global merit function does not affect our results for the other parameters. Because of the lower number of constrained eccentricities in our sample, we do not attempt to improve the description of the eccentricity distribution by testing different forms for $pdf(e)$.

C. On the determination of binary interaction rates

In this section we determine the relative frequencies of binary interaction scenarios and describe assumptions adopted in the construction of Figure 2. All fractions are expressed with respect to the number of all stars born as O-type stars, including primaries, secondaries and single stars. We ignore lower mass stars that may become O stars during their life by gaining mass via mass accretion or via a binary merger. We also ignore triple and higher order multiple systems.

C.1. Initial conditions

We adopt a Kroupa initial mass function (IMF, 41) for the primary stars. We adopt a mass range of 15 to 60 solar masses for O stars, in agreement with our observed sample and with recent calibrations of O-type stellar parameters (1). The derived fractions discussed below are not sensitive to the slope of the IMF because the considered mass range is fairly limited. Orbits are assumed to be circular, which results in a lower limit to the estimated fraction of interacting binaries as eccentric orbits may facilitate interaction during periastron passage. We discuss this assumption in §C.4 below.

We adopt the intrinsic distribution of orbital periods and mass ratios obtained in this work as the initial conditions, i.e. as the distributions on the zero-age main sequence. A fraction f_{bin} of the objects are binaries with at least one O-star. Initial mass ratios range from 0.1 to 1.0 and initial periods from $10^{0.15}$ to $10^{3.5}$ days (Table S3). We find that 37% of binaries are O+O systems, in excellent agreement with the observed sample.

An intrinsic binary fraction f_{bin} of 0.69 implies that 75% of all stars born as O stars are, at birth, in a binary system with $P < 10^{3.5}$ days and $q > 0.1$. The remaining 25% are assumed to be effectively single, even though part of these may have a nearby very low mass companion ($q < 0.1$), or a companion in a very wide orbit ($P > 10^{3.5}$ days).

C.2. Fraction of stars that interact with a companion

The initial orbital period is the main parameter which determines whether and when a binary interacts by mass transfer. We adopt a maximum limit of 1500 days for the orbital period below which significant interaction occurs (6, 8), which corresponds to the approximate limit for the initially most massive star to lose nearly its entire hydrogen-rich envelope before the supernova explosion. For primary masses between 15 and 25 solar masses this limit is a conservative estimate. When the primary star becomes a red supergiant, systems with periods up to about 10 years (~ 3500 days) may still interact by formation and subsequent ejection of a common envelope. For systems with more massive primaries, i.e. over about 30 solar masses, the maximum orbital period is uncertain because such stars experience significant mass loss, by stellar winds (42-43) and eruptions (44), which may prevent them from reaching red supergiant dimensions. A companion in a wide orbit may accrete a small fraction of the wind of the star and shape the circumstellar medium around it but no interaction in the form of Roche lobe overflow (RLOF) is expected. The initial mass function favors less massive systems for which our limiting period leads to a conservative estimate of the fraction of interacting systems. More importantly, the distribution of orbital periods is dominated by the short-period systems so that the exact location of the maximum period at which systems interact has no impact on the rates discussed below.

We find that $71 \pm 8\%$ of all stars born as O-stars are a member of a binary system that will interact by Roche lobe overflow, which significantly alters the further evolution and final fate of both stars. The uncertainty is dominated by the allowed range in the intrinsic binary fraction.

C.3. The time of interaction

To further estimate the type of interaction that the stars experience we separate the short period systems for which mass-transfer starts during the main sequence evolution of the primary star (case A) from the wider systems, in which interaction starts as the primary expands on its way to the red supergiant phase (case B) or later (case C). The limiting orbital period distinguishing case A from case B and C depends on the maximum radii that massive stars reach during their main sequence evolution which is affected by uncertainties in the treatment of convection. The typical limiting orbital period found in binary evolutionary models is about five days (27, 28). Recent efforts to calibrate stellar models of massive stars against observations result in larger maximum radii (3) which imply a limiting orbital period 50% larger. We adopt a limit of six days which yields a conservative prediction of the fraction of case A interactions and, therefore, of mergers (see below).

These assumptions imply that $26 \pm 7\%$ of all stars born as O-type are a member of a binary system that will interact by case A mass transfer during their main sequence (Fig. 2). The error bar reflects the uncertainty in the binary fraction and the distribution of orbital periods. Secondary stars are, by definition, initially less massive than their primary counterpart and thus evolve more slowly. In many of the wider systems, case B

and C mass transfer begins thus when the secondary is still a main sequence star. This adds a fraction of about 12% to the number of O stars which interact during the main sequence. In total, we estimate the fraction of all stars born as O-type that will experience interaction before leaving the main sequence to be close to 40%. The evolution of these stars is affected at an early stage, with consequences for their entire further evolution.

C.4. The fraction of stars that merge

A large fraction of the very close binaries is expected to merge. In case A systems we estimate this fraction based on the results of detailed binary evolutionary calculations (29). These models show that stars in binary systems with mass ratios or periods beyond certain critical limits evolve into deep contact quickly after the onset of mass transfer. Although the evolution during this contact phase is not well understood it is anticipated that dissipative processes and the loss of mass with high angular momentum through the outer Lagrangian point drive the stars deeper into contact and lead to the coalescence of both stars. Albeit in a lower mass system, direct evidence for the occurrence of merging comes from the detection of a contact binary with a shrinking orbit as the progenitor of the transient event V1309 Sco (45).

Typical values for the critical period and mass-ratio below which O-type binaries merge are $P < 2$ days and $q < 0.65$, respectively, although these values are affected by considerable uncertainties (46). Under these assumptions we find that 20% of all O-type stars will merge, during their main-sequence lifetime, with another main sequence star. We estimate an uncertainty of $\pm 5\%$ on the rate of mergers by varying the assumed critical mass ratio from 0.4 to 0.75 and of $\pm 4\%$ by varying the critical period between 1.5 and 3 days. Uncertainty resulting from the assumed initial distribution functions is dominated by the uncertainty in the period distribution function, which amounts to a variation of $\pm 5\%$ as well.

We also expect a significant number of mergers between an evolved star and a main sequence star (case B and C mergers). Although the binary separation is larger at the start of the interaction compared to case A RLOF, the higher mass transfer rates lead to more violent interaction. Resulting mass and angular momentum loss from the system can drive the two stars together. Unfortunately, the rates of these mergers are subject to much larger uncertainties than those resulting from case A interaction. We adopt the results of the simulations by Podsiadlowski et al. (6) who find that about 13% of all case B and C systems merge. Applying this to our fraction of binaries with orbital periods between 6 to 1500 days, we find that an additional 4% of all stars born as O stars merge. The dependence of the case B and C merger rate on orbital period is however uncertain. The shape of the corresponding area in Figure 2 is only a schematic representation. We assume that systems with orbital period longer than 500 days eject the common envelopes and do not merge. In shorter period systems we assume that extreme mass-ratio systems will merge, independently of the orbital period. As a consequence only O stars that are primaries are affected. Finally, the simulations by Podsiadlowski et al. use a distribution of orbital periods that does not include the strong preference for short period

systems obtained in this work. The fraction of case B and C mergers is possibly larger than we calculate here.

We assume circular orbits even though a fraction of our systems (25 to 50% given the uncertainties in η) have eccentricities larger than 0.3. These systems might interact earlier than discussed here as a result of preferential interaction at periastron passage. However, all very short period ($P < 2$ days) systems have a zero eccentricity and all systems with $P < 6$ days have $e \leq 0.3$ (Fig. S1). Because these systems are unaffected by observational biases (Fig. 2) it is reasonable to assume that there are no short period highly eccentric systems. This therefore does not affect our estimate of case A mergers and, because case A RLOF is the dominant contribution to the total number of mergers, implies that the total fraction of mergers cannot be strongly overestimated either.

To summarize, we find that 20% of all stars born as O stars will merge as a result of case A mass transfer and another 4% as a result of case B and C mass transfer. Given the uncertainties discussed, we estimate a combined fraction of 20-30% of all stars born as O-stars to merge with their companion.

C.5. Mass stripping, accretion and spin-up

In binaries with periods shorter than 1500 days, whenever binary interaction does not lead to an irreversible shrinkage of the orbit and a merger, the components of the binary interact through RLOF and the primary is stripped of its hydrogen-rich envelope. We find that one third of all stars born as O-stars undergo such stripping and lose enough of their hydrogen-rich envelope that they explode as hydrogen-deficient supernovae (type Ib / Ic / IIb).

A fraction of the mass lost by the donor is accreted by the companion star which gains mass and angular momentum. Because of the high specific angular momentum of such material the accretion of just a few percent of the mass lost by the primary will spin up the secondary star to its critical rotational velocity. This process affects about 14% of the stars born as O stars, most of which will experience accretion and spin-up. An exception to this scenario are the secondary stars in the widest systems. In these systems, the primaries develop a cool, convective envelope before RLOF begins which may lead to the formation of a common envelope on such short time scales that the companion star has no time to accrete a significant amount of material. These systems are the progenitors of X-ray binaries which host a neutron star or black hole that originates from the core of the original primary star and accretes material from the secondary star.

The main uncertainty in the interaction fractions derived in this section depends on the uncertain fraction of systems that merge. In most cases, a failed merger leads to mass stripping of the primary and accretion by the secondary as described above. These uncertainties do not modify the number of objects for which evolution is strongly affected by binary interaction and thus our main conclusions are unaffected.

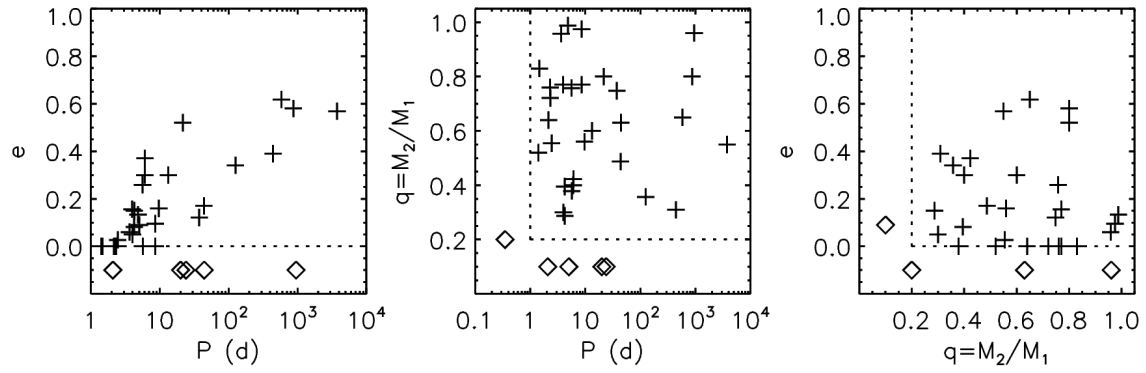


Fig. S1.

Our sample binaries in the orbital period P - mass ratio q - eccentricity e planes (crosses). Diamonds indicate systems for which only one of the two parameters is known: they are plotted in parts of the graphs where no systems are found and are separated from the rest of the parameter space by dashed lines.

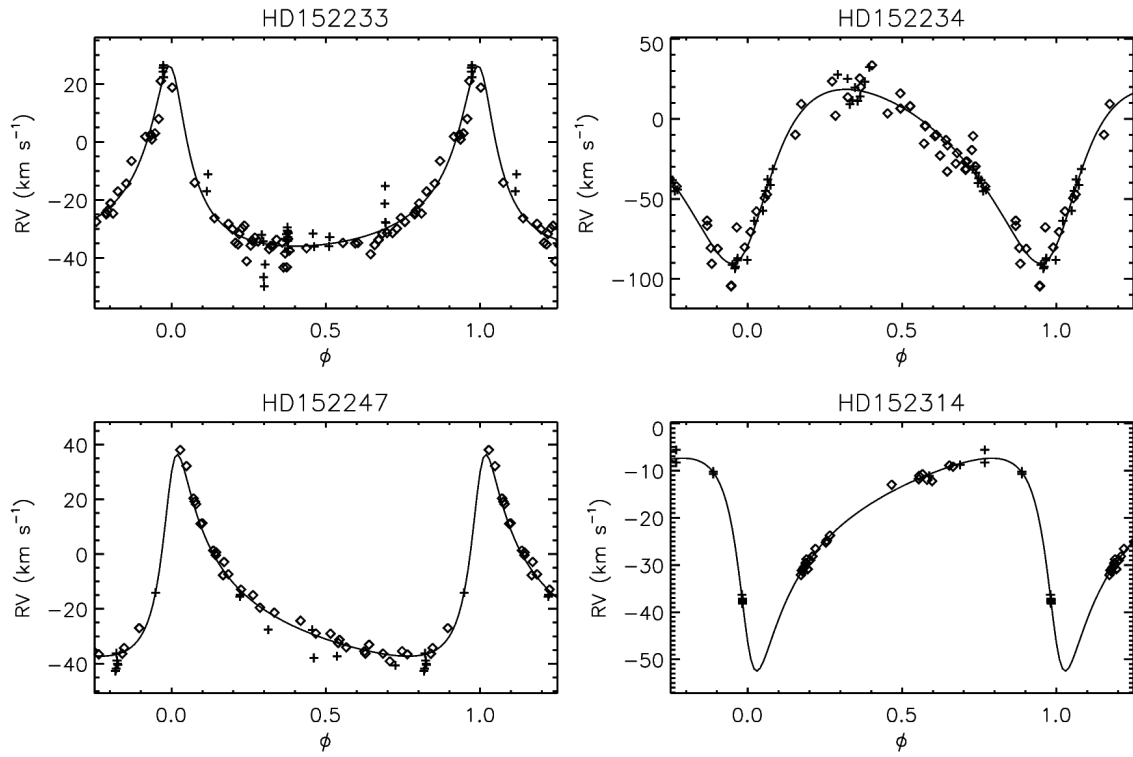


Fig. S2

Previously published and new RV measurements (crosses and circles, respectively) and best-fit RV-curves (solid line) of four long period spectroscopic binaries in our sample. The best-fit orbital elements are given in Table S2.

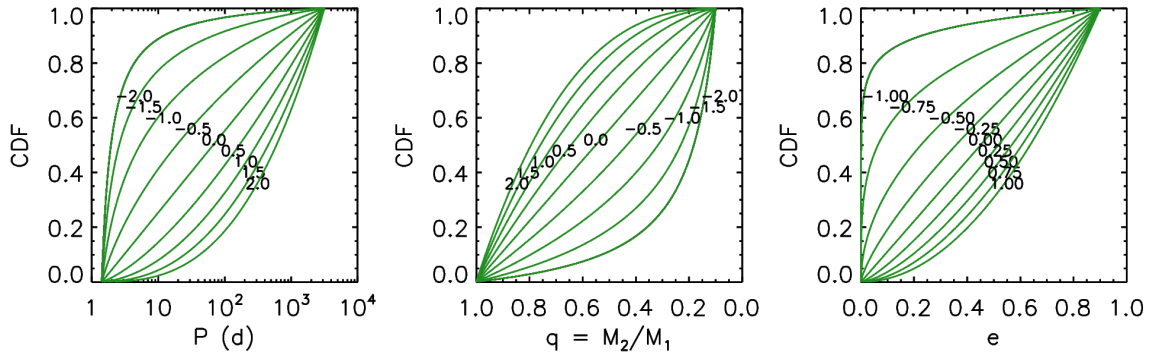


Fig. S3

Period, mass-ratio and eccentricity cumulative distribution functions (*CDFs*) for different values of the power-law exponent as indicated by the labels in each plot. The displayed ranges correspond to those explored in our simulations but, for clarity, not all the intermediate steps are shown (see Table S3).

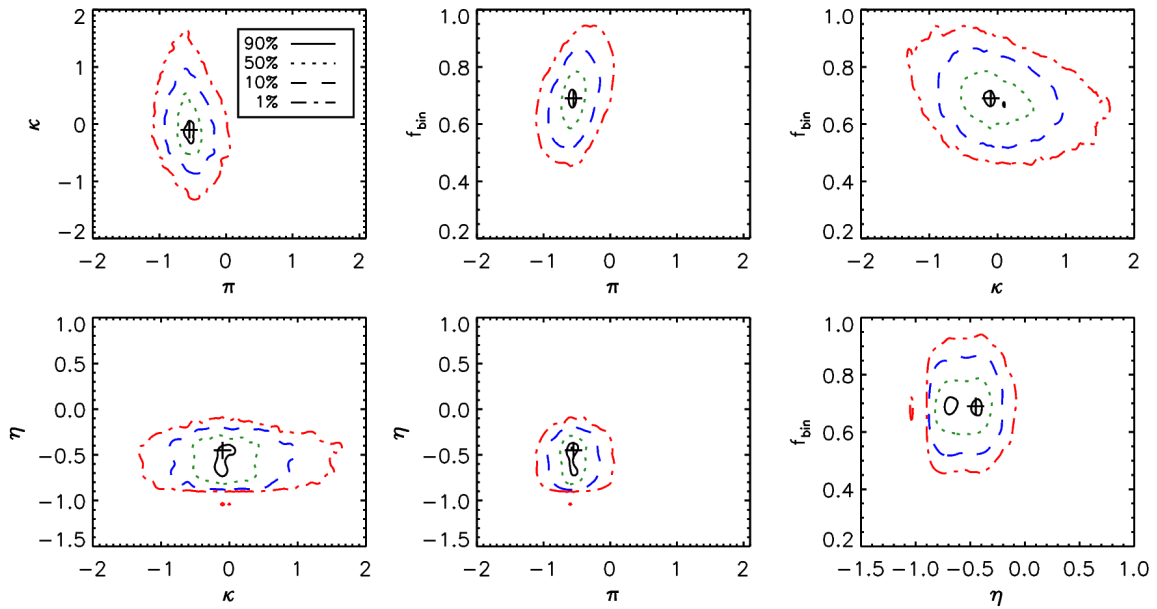


Fig. S4

Projection of the global merit function Ξ over the six two-by-two planes defined by our four degrees of freedom. The curves represent loci of equal merit, with levels of 0.9, 0.5, 0.1 and 0.01 times the maximum value of Ξ . The cross (+) shows the position of the absolute maximum.

Table S1.

Notation used in this paper

Symbol	Definition
pdf	Probability density function
CDF	Cumulative distribution function
f_{obs}	Observed binary fraction
f_{bin}	Intrinsic binary fraction
ϕ_{tr}	True anomaly
ϕ	Orbital phase
P	Orbital period
e	Orbital eccentricity
T	Time of periastron passage
ω	Argument of the periastron
i	Orbital inclination
γ	Systemic velocity
v	Projected orbital velocity
t	Time of the observation
M	Stellar mass
q	Secondary to primary mass-ratio (M_2/M_1)
G	Gravitational constant

Table S2.

Best fit orbital solution of the four long period systems of Figure S2.

Orbital parameter	HD152233	HD152234	HD152247	HD152314
P (day)	868.61 ± 3.20	125.135 ± 0.050	582.84 ± 1.00	3710 ± 95
e	0.58 ± 0.03	0.34 ± 0.03	0.62 ± 0.02	0.57 ± 0.04
γ (km s ⁻¹)	-22.5 ± 0.6	-21.3 ± 1.2	-19.3 ± 0.6	-20.5 ± 0.4
K_1 (km s ⁻¹)	31.1 ± 2.9	53.9 ± 1.7	36.8 ± 2.0	22.5 ± 2.5
T (HJD-2 400 000)	56281.66 ± 0.96	56043.46 ± 2.11	56151.07 ± 6.36	56910 ± 109
ω (°)	11.8 ± 2.9	220.6 ± 6.1	326.1 ± 2.0	137.4 ± 5.2
r.m.s. (km s ⁻¹)	4.6	9.5	3.1	0.8

Table S3.

Parameters (Col.1) and corresponding probability density functions (*pdf*) (Col.2), considered parameter space (Col.3), variables (Col.4), investigated ranges of the power law exponents π , κ and η and of the intrinsic binary fraction (Col.5) and step sizes (Col.6).

Parameter	<i>pdf</i>	Domain	Variable	Range	Step
$\log_{10}(P/\text{day})$	$(\log_{10} P)^\pi$	0.15 – 3.5	π	-2.00 – +2.00 -0.80 – -0.20	0.10 0.05
q	q^κ	0.1 – 1.0	κ	-2.00 – +2.00 -0.50 – +0.50	0.10 0.05
e	e^η	0.0 – 0.9	η	-1.50 – +1.00 -0.80 – -0.20	0.10 0.05
f_{bin}	n/a	n/a	f_{bin}	0.20 – 1.00 0.50 – 1.00	0.05 0.01

Table S4.

Orbital properties of the binaries in our sample. Unconstrained parameters are indicated by '-'.

Object	Cluster	SB1/SB2	Spectral Type	P (day)	$q=M_2/M_1$	e	Reference
BD+60497	IC1805	SB2	O6V+O8V	3.9586	0.77	0.16	17
BD+60513	IC1805	SB2	O7.5V	–	–	–	17
HD15558	IC1805	SB2	O5.5III+O7III	442	0.31	0.39	16
HD17505Aa	IC1848	SB2	O7V((f))+O7V((f))	8.571	0.98	0.10	17
HD17520	IC1848	SB1	O8V	–	–	–	17
BD60594	IC1848	SB1	O8.5Vn	20:	–	–	17
DN Cas	IC1805	SB2	O8V+B0.2V	2.31	0.72	0.00	17
HD93161A	Tr16	SB2	O8V+O9V	8.57	0.77	0.00	47
HD93161B	Tr16	SB1	O6.5V(f)	–	–	–	47
HD93205	Tr16	SB2	O3V+O8V	6.08	0.42	0.37	48
V662Car	Tr16	SB2	O5.5Vz+O9.5V	1.41356	0.52	0.00	49
HD93130	Tr16	SB1	O6III(f)	23.944	–	–	50
CPD-592603	Tr16	SB2	O7V+O9.5V	2.15287	0.64	0.00	51
CPD-592628	Tr16	SB2	O9.5V+B0V	1.469332	0.83	0.00	52, 53
HD93343	Tr16	SB2	O8+O8	44.15	0.63	–	20
CPD-592636AB	Tr16	SB2	O7V+O8V	3.63284	0.96	0.06	54
CPD-592636C	Tr16	SB1	O9V	5.034	–	0.09	54
CPD-592635	Tr16	SB2	O8V+O9.5V	2.29995	0.76	0.00	55
CPD-592641	Tr16	SB2	O5.5-O6V((f+?p))+B2V-II	14.257	0.29	0.15	20
HD101131	IC2944	SB2	O6.5V((f))+O8.5V	9.65	0.56	0.16	56
HD101190	IC2944	SB2	O4V((f))+O7V	6.05	0.40	0.30	21
HD101191	IC2944	SB1	O8V	–	–	–	21
HD101205	IC2944	SB1	O7III _n ((f))	2.080	–	–	21
HD101413	IC2944	SB2	O8V+B3:V	–	0.20	–	21
HD101436	IC2944	SB2	O6.5V+O7V	37.37	0.75	0.12	21
HD100099	IC2944	SB2	O9III+O9.7V	21.560	0.80	0.52	21
HD308813	IC2944	SB2	O9.5V	–	–	–	21
CPD-417742	NGC6231	SB2	O9V+B1.5V	2.4407	0.55	0.03	57
HD152219	NGC6231	SB2	O9.5III+B1-2V/III	4.2403	0.40	0.08	58
HD152248	NGC6231	SB2	O7.5III(f)+O7III(f)	4.8216	0.99	0.13	18
HD152218	NGC6231	SB2	O9IV+O9.7V	5.6039	0.76	0.26	59
CPD-417733	NGC6231	SB2	O8.5V+B3	5.6815	0.38	0.00	60
HD152234	NGC6231	SB2	O9.7I+B1-3:	125.135	0.36	0.34	This work
HD152233	NGC6231	SB2	O5.5III(f)+O7.5III/V	868.61	0.80	0.58	This work
HD152314	NGC6231	SB2	O8.5V+B1-3V	3710	0.55	0.57	This work

HD152247	NGC6231	SB2	O9III+O9.7V	582.84	0.65	0.62	This work
HD168075	NGC6611	SB2	O6.5V((f))+B0.5V	43.6	0.49	0.17	61
HD168137	NGC6611	SB2	O7V+O8V	912	0.96	–	This work
HD168183	NGC6611	SB2	O9.5III+B3-5V/III	4.015	0.30	0.05	19
BD-134923	NGC6611	SB2	O4V((f+))+O7.5V	13.30	0.60	0.30	19